
SAMPLE AND MAP FROM A SINGLE CONVEX POTENTIAL: GENERATION USING CONJUGATE MOMENT MEASURES

Nina Vesseron
CREST-ENSAE, IP Paris
nina.vesseron@ensae.fr

Louis Béthune
Apple
l_bethune@apple.com

Marco Cuturi
CREST-ENSAE, Apple
cuturi@apple.com

ABSTRACT

A common approach to generative modeling is to split model-fitting into two blocks: define first *how* to sample noise (e.g. Gaussian) and choose next *what* to do with it (e.g. using a single map or flows). We explore in this work an alternative route that *ties* sampling and mapping. We find inspiration in *moment measures* (Cordero-Erausquin and Klartag, 2015), a result that states that for any measure ρ supported on a compact convex set of \mathbb{R}^d , there exists a unique convex potential u such that $\rho = \nabla u \# e^{-u}$. While this does seem to tie effectively sampling (from log-concave distribution e^{-u}) and action (pushing particles through ∇u), we observe on simple examples (e.g., Gaussians or 1D distributions) that this choice is ill-suited for practical tasks. We study an alternative factorization, where ρ is factorized as $\nabla w^* \# e^{-w}$, where w^* is the convex conjugate of w . We call this approach *conjugate moment measures*, and show far more intuitive results on these examples. Because ∇w^* is the Monge map between the log-concave distribution e^{-w} and ρ , we rely on optimal transport solvers to propose an algorithm to recover w from samples of ρ , and parameterize w as an input-convex neural network.

1 Introduction

A decade after the introduction of GAN (Goodfellow et al., 2014) and VAE (Kingma and Welling, 2014), the field of generative modeling has grown into one of the most important areas of research in machine learning. Both canonical approaches follow the template of learning a transformation that can map random codes to meaningful data. These transformations can be learned in supervised manner, as in the dimensionality reduction pipeline advocated in VAEs, or distributionally as advocated in the purely generative literature. In the latter, the variety of such transforms has gained remarkably in both complexity, using increasingly creative inductive biases, from Neural-ODEs (Chen et al., 2018; Grathwohl et al., 2018), diffusions (Song et al., 2020; Ho et al., 2020), optimal transport (Korotin et al., 2020) to flow-matching (Lipman et al., 2023; Tong et al., 2023; Pooladian et al., 2023).

Sample first, move next. All of these approaches share, however, a standard Gaussian multivariate distribution to generate noise/codes. For both GANs and VAEs, that choice is usually made because of its simplicity, but also, in the case of diffusion models, because Gaussian distributions can be recovered quickly with suitable stochastic processes (Ohrstein-Uhlenbeck). Other works have considered optimizing prior noise distributions (Tomczak and Welling, 2018; Lee et al., 2021; Liang et al., 2022) but still do so in a two step approach where mappings are estimated independently. We propose in this work a new approach where sampling and transforms are not treated separately, but seen as two facets of the same single object.

Tying sampling and action. Our work looks to *moment measures* Cordero-Erausquin and Klartag (2015) to find inspiration for a factorization that ties both sampling and action. (Cordero-Erausquin and Klartag, 2015) proved that for any sufficiently regular probability measure ρ , one can find an essentially-continuous, convex potential u such that

$\rho = \nabla u \# e^{-u}$: essentially, *any* probability distribution can be recovered by first sampling points from a log-concave distribution e^{-u} , and moving them with ∇u where, remarkably, the *same* single convex potential u is used twice.

Our Contributions. We build on the work of Cordero-Erausquin and Klartag (2015) to propose an alternative path to build generative models, that we call *conjugate moment measures*.

- After recalling in detail the contribution of Cordero-Erausquin and Klartag (2015) in §2.1, we argue in §3.1 that the moment measure factorization may not be suitable for practical tasks. For instance, in the case of Gaussian distributions, we show that if ρ is Gaussian with variance Σ , the corresponding log-concave distribution e^{-u} is Gaussian with variance Σ^{-1} , amplifying beyond necessary any minor degeneracy in Σ . Similarly, for univariate ρ , we found that the spread of e^{-u} is inversely proportional to that of ρ . While these results are not surprising from a theoretical perspective, they suggest a different strategy to estimate a tied sample/action factorization.
- We propose instead in §3.2 a new factorization that is conjugate to that of Cordero-Erausquin and Klartag (2015): We show that any absolutely continuous probability distribution ρ supported on a compact convex set can be written as $\rho = \nabla w^* \# e^{-w}$, where w^* is the convex conjugate of w . Importantly, in our factorization the convex potential w is used to map ρ to e^{-w} , since one has equivalently that $\nabla w \# \rho = e^{-w}$. Note that evaluating w^* , the convex conjugate of w , only requires solving a convex optimization problem, since w is assumed to be convex.
- We explore how to infer the potential w arising from the conjugate factorization above using only samples from ρ , by relying on optimal transport (OT) theory (Santambrogio, 2015). Indeed, since the condition $\rho = \nabla w^* \# e^{-w}$ is equivalent to stating that w^* is the Brenier potential linking e^{-w} to ρ , we can parameterize w as an input-convex neural network w_θ whose gradient is an OT map. We provide illustrations on simple generative examples.

2 Background

We present neural approaches to solve the OT problem and introduce moment measures.

2.1 Optimal Transport

Let $\mathcal{P}(\mathbb{R}^d)$ be the set of Borel probability measures on \mathbb{R}^d . Let $\mu, \nu \in \mathcal{P}(\mathbb{R}^d)$ and set $\Pi(\mu, \nu)$ to be the set of couplings between μ and ν . We consider the primal OT problem with squared-Euclidean cost,

$$\mathcal{W}_2^2(\mu, \nu) := \inf_{\pi \in \Pi(\mu, \nu)} \int_{\mathbb{R}^d \times \mathbb{R}^d} \frac{1}{2} \|x - y\|^2 d\pi(x, y). \quad (1)$$

This problem admits a dual formulation:

$$\begin{aligned} & \sup_{(f, g) \in L^1(\mu) \times L^1(\nu)} \int_{\mathbb{R}^d} f(x) d\mu(x) + \int_{\mathbb{R}^d} g(y) d\nu(y), \\ & \text{s.t. } f(x) + g(y) \leq \frac{1}{2} \|x - y\|^2, \forall (x, y) \in \mathbb{R}^d \times \mathbb{R}^d. \end{aligned} \quad (2)$$

The functions f and g that maximize the expression in equation 2 are referred to as the Kantorovich potentials. Equation 1 can itself be seen as a relaxation of the Monge formulation of the OT problem,

$$\inf_{\substack{T: \mathbb{R}^d \rightarrow \mathbb{R}^d, \\ T \# \mu = \nu}} \int_{\mathbb{R}^d} \frac{1}{2} \|x - T(x)\|^2 d\mu(dx) \quad (3)$$

where $\#$ is the pushforward operator. An important simplification of equation 2 comes from the knowledge that solutions f^*, g^* for equation 2 must necessarily be such that $\frac{1}{2} \|\cdot\|^2 - f^*$ is convex. Using this parameterization, let $\mathcal{C}(\mathbb{R}^d)$ be the space of convex functions in \mathbb{R}^d . Brenier (1991) proved that in that case, T^* solving equation 3 exists, and is given by the gradient of the convex function $\frac{1}{2} \|\cdot\|^2 - f^*$, namely $\text{Id} - \nabla f^*$. Making a change of variables, $u = \frac{1}{2} \|\cdot\|^2 - f$ and using the machinery of cost-concavity (Santambrogio, 2015, §1.4), one can show that solving equation 2 is equivalent to computing the minimizer of:

$$\min_{\substack{u \in \mathcal{C}(\mathbb{R}^d) \\ u(0)=0}} \mathcal{T}_u(\mu, \nu) := \int_{\mathbb{R}^d} u(x) d\mu(x) + \int_{\mathbb{R}^d} u^*(x) d\nu(x) \quad (4)$$

where $u^*(y) := \max_{x \in \mathbb{R}^d} \langle x, y \rangle - u(x)$ is the convex-conjugate of u and noting that we lift any ambiguity on u by selecting the unique potential such that $u(0) = 0$. By denoting $\mathcal{T}(\mu, \nu)$ the optimal value and $\mathfrak{B}(\mu, \nu)$ the Brenier potential solving equation 4 above, this results in $\nu = \nabla \mathfrak{B}(\mu, \nu) \# \mu$.

Neural OT solvers. The goal of neural OT solvers is to estimate $\mathfrak{B}(\mu, \nu)$ using samples drawn from the source μ and the target distribution ν . Makkuva et al. (2020); Korotin et al. (2020) proposed methods that leverage input convex neural networks (ICNN), originally introduced by Amos et al. (2017), to parameterize the potential u as an ICNN. A key challenge in these approaches is managing the Legendre transform u^* . To overcome this, a surrogate network can be employed to approximate u^* with recent advances by Amos (2023) improving these implementations through amortized optimization.

2.2 Moment Measures

For a given convex function u , the moment measure of u is defined as the pushforward measure $\nabla u \# \mathfrak{P}_u$ where \mathfrak{P}_u is the (Gibbs) log-concave probability measure with density

$$\mathfrak{P}_u(x) := \frac{e^{-u(x)}}{\int_{\mathbb{R}^d} e^{-u(z)} dz}. \quad (5)$$

The moment measure of u is in particular well defined when the quantity $\int_{\mathbb{R}^d} e^{-u(z)} dz$ is positive and finite.

While any measure ρ supported on a compact set K is guaranteed to be the moment measure of some convex potential u (Santambrogio, 2016), Cordero-Erausquin and Klartag showed that u is often discontinuous at the boundary ∂K . In Cordero-Erausquin and Klartag (2015), they studied the variational problem

$$\min_{u \in \mathcal{C}(\mathbb{R}^d)} \int u^* d\rho - \ln \left(\int e^{-u} \right), \quad (6)$$

and proved that if ρ is a probability measure with a finite first moment, whose barycenter is at 0 and is not supported on a hyperplane, then it is the moment measure of an essentially continuous potential. Subsequently, Santambrogio (2016) derived the same result using a variational formulation over probability measures, given by

$$\min_{\xi \in \mathcal{P}(\mathbb{R}^d)} \{ \mathcal{E}(\xi) + \mathcal{T}(\xi, \rho) : \xi \in \mathcal{P}_1(\mathbb{R}^d) \}, \quad (7)$$

where \mathcal{E} denotes the negative Shannon entropy of a measure, and $\mathcal{T}(\xi, \rho)$ refers to the optimal value of equation 4. When ρ meets the conditions enunciated in Cordero-Erausquin and Klartag (2015), Santambrogio showed that the minimizers of equation 7 coincide with the Gibbs distributions \mathfrak{P}_u , where u are the convex functions whose moment measure is ρ .

3 Conjugate Moment Measures

We denote the convex function u whose moment measure is ρ as the moment *potential* of the distribution ρ . Additionally, we refer to the Gibbs distribution associated with such potential, \mathfrak{P}_u as in equation 5, as the *Gibbs factor* of ρ .

3.1 Limitations of Moment Measures

The general case By rewriting the KL divergence between ρ and \mathfrak{P}_{u^*} as follows:

$$\text{KL}(\rho \parallel \mathfrak{P}_{u^*}) = \mathcal{E}(\rho) + \int u^* d\rho + \ln \left(\int e^{-u^*} \right),$$

and applying this in the variational problem studied by Cordero-Erausquin and Klartag as referenced in equation 6, we obtain that the moment potentials of ρ minimize the following problem:

$$\min_{u \in \mathcal{C}(\mathbb{R}^d)} \text{KL}(\rho \parallel \mathfrak{P}_{u^*}) - \ln \left(\int e^{-u} \int e^{-u^*} \right). \quad (8)$$

The quantity $\int e^{-u} \int e^{-u^*}$ is intrinsic to the density \mathfrak{P}_u , and has been investigated by Ball (1986) and Artstein-Avidan et al. (2004) who demonstrated that, up to a translation, this term is maximized when \mathfrak{P}_u is Gaussian. This reformulation reveals that the Gibbs distributions associated with the Legendre transform of ρ 's moment potentials, \mathfrak{P}_{u^*} , are the closest log-concave distribution to ρ , adjusted by the regularization term $\int e^{-u} \int e^{-u^*}$. As a result, the Gibbs factor of ρ may differ significantly from ρ , especially in cases where ρ is a Gaussian distribution.

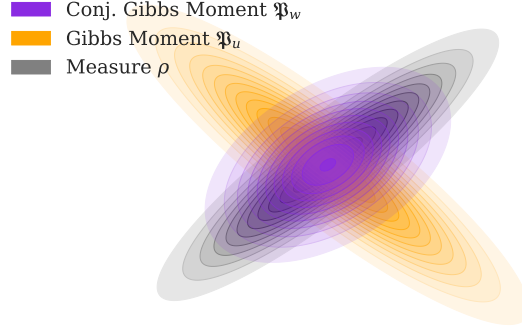


Figure 1: **Gibbs factor** and **conjugate Gibbs factor** of $\rho = \mathcal{N}\left(0, \begin{bmatrix} 2 & 1.8 \\ 1.8 & 2 \end{bmatrix}\right)$.

Gaussian distributions. The multivariate normal distribution $\mathcal{N}(m, \Sigma)$ with Σ non-degenerate is recovered as by \mathfrak{P}_v with $v(x) = \frac{1}{2}(x - m)^T \Sigma^{-1}(x - m)$. When $m \neq 0$ or Σ is degenerate, Cordero-Erausquin and Klartag show that $\mathcal{N}(m, \Sigma)$ is not a moment measure. Yet, when Σ is non-degenerate, moment potentials of $\mathcal{N}(0, \Sigma)$ exist and have an analytical expression given by the following proposition.

Proposition 1. *Let $\rho = \mathcal{N}(0_{\mathbb{R}^d}, \Sigma)$. If Σ is non degenerate, the moment potential of ρ is*

$$u_m(x) = \frac{1}{2}(x - m)^T \Sigma(x - m),$$

for some $m \in \mathbb{R}^d$. The Gibbs factor of ρ is $\mathcal{N}(m, \Sigma^{-1})$.

The proof is provided in the Appendix and relies on the fact that the OT map between two Gaussians is known in closed form Peyré et al. (2019). Intuitively this results can be interpreted as follows. When a peaked distribution ρ is centered around the origin (e.g. $\Sigma \approx 0$), its corresponding moment potential is such that the *image* set ∇u on the support of \mathfrak{P}_u is necessarily tightly concentrated around 0. This has the implication that u is a *slowly* (almost constant) varying potential on the entire support of \mathfrak{P}_u . As a result, one has the (perhaps) counter-intuitive result that the more peaky ρ , the more spread-out \mathfrak{P}_u must be. From this simple observation, validated experimentally in Section 3.3 we draw the intuition that a change is needed to reverse this relationship, while still retaining the interest of a measure factorization result.

3.2 Adding a Conjugate

Our main theorem is stated as follows:

Theorem 1. *Let ρ be an absolutely continuous probability measure supported on a compact, convex set. Then, there exists a convex function w such that*

$$\rho = \nabla w^* \# \mathfrak{P}_w.$$

Similarly to the terminology we used for moment measures, we refer to ρ as the *conjugate moment measure* of w , the potential w as the *conjugate moment potential* of ρ , and \mathfrak{P}_w as ρ 's *conjugate Gibbs factor*.

Proof Sketch. The complete proof, along with the theorems used in the proof, can be found in the Appendix. We rely on the identity $\nabla w^* \circ \nabla w = \text{id}$ that holds for strictly convex functions w and show the existence of a strictly convex potential w that verifies $\nabla w \# \rho = \mathfrak{P}_w$. To proceed, we first introduce some notations. Let $\mathcal{L}(\mathbb{R})$ be the set of functions mapping \mathbb{R}^d to $\mathbb{R} \cup \{+\infty\}$. Given a non-negligible set $\Omega \subset \mathbb{R}^d$ and a continuous function $v : \Omega \rightarrow \mathbb{R}$ such that $\int_{\mathbb{R}^d} e^{-v(z)} dz$ is finite, we denote by \mathfrak{P}_v^Ω the probability measure with density

$$\frac{e^{-v(x)} \mathbf{1}_{x \in \Omega}}{\int_{\Omega} e^{-v(z)} dz}.$$

We then define, for a probability ρ supported on a non-negligible set Ω , the map $G_\rho^\Omega : \mathcal{L}(\mathbb{R}) \rightarrow \mathcal{L}(\mathbb{R})$ which to a potential v associates the Brenier potential, defined in equation 4, from ρ to \mathfrak{P}_v^Ω

$$G_\rho^\Omega(v) := \mathfrak{B}(\rho, \mathfrak{P}_v^\Omega)$$

The fixed points of G_ρ^Ω are precisely the convex functions v such that $\nabla v \# \rho = \mathfrak{P}_v^\Omega$ from which we can construct w defined as $w(x) = v(x)$ for $x \in \Omega$ and $w(x) = +\infty$ elsewhere. This function w is convex and verifies $\nabla w \# \rho = \mathfrak{P}_w$ (since ρ is supported on Ω). We rely on Schauder's fixed point theorem to show that G_ρ^Ω admits a fixed-point. Given a Banach space $(X, \|\cdot\|)$ and a compact, convex and nonempty set $\mathcal{M} \subset X$, Schauder's theorem states that any continuous operator $A : \mathcal{M} \rightarrow \mathcal{M}$ has at least one fixed point. In this proof, we consider the Banach space of continuous functions over a compact set Ω , denoted $\mathcal{C}(\Omega)$, equipped with the supremum norm, and establish the following theorem that directly implies Theorem 1.

Theorem 2. *Let ρ be an absolutely continuous probability measure supported on a compact, convex set $\Omega \subset \mathbb{R}^d$. Then G_ρ^Ω admits a fixed point in*

$$\mathcal{M} = \{f \in \mathcal{C}(\Omega) \text{ such that } \forall x, y \in \Omega, \\ |f(x) - f(y)| \leq R\|x - y\|_2 \text{ and } f(0_{\mathbb{R}^d}) = 0\}$$

where R is the radius of an euclidean ball that contains Ω i.e., $\Omega \subset \mathcal{B}(0, R) = \{x \in \mathbb{R}^d, \|x\|_2 \leq R\}$.

We first show that the set \mathcal{M} is a non-empty, compact, convex set of $X = (\mathcal{C}(\Omega), \|\cdot\|_\infty)$ by relying Arzela-Ascoli's theorem for the compactness. We then use Brenier's theorem that, given the absolute continuity of ρ , guarantees the existence of the Brenier potential $\mathfrak{B}(\rho, \mathfrak{P}_v^\Omega)$ and the fact that G_ρ^Ω is therefore well-defined on the set $\mathcal{M} \subset \mathcal{C}(\Omega)$. Moreover, the gradient of the obtained potential $G_\rho^\Omega(v)$ transports ρ on \mathfrak{P}_v^Ω which is compactly supported on $\Omega \subset \mathcal{B}(0, R)$. For this reason, $\nabla G_\rho^\Omega(v)$ is bounded by R on Ω and the obtained potential is Lipschitz continuous with constant R . This permits to show that $G_\rho^\Omega(\mathcal{M}) \subseteq \mathcal{M}$. To prove the continuity of G_ρ^Ω on \mathcal{M} , one can remark that $G_\rho^\Omega = H_\rho \circ F^\Omega$, with $F^\Omega(v) = \mathfrak{P}_v^\Omega$ and $H_\rho(\mu) = \mathfrak{B}(\rho, \mu)$, both viewed as functions from $\mathcal{C}(\Omega)$ to $\mathcal{C}(\Omega)$. To show that F^Ω is continuous, we use the definition of continuity in $X = (\mathcal{C}(\Omega), \|\cdot\|_\infty)$ while we rely on Theorem 1.52 from Santambrogio (2015) to prove that H_ρ is continuous. We conclude by applying Schauder's theorem.

3.3 Illustrations

We focus on the case where ρ is Gaussian to verify that our conjugate factorization has better properties. Recall that we saw in subsection 3.1 that Gibbs factors of $\mathcal{N}(0, \Sigma)$ were multivariate normal distributions with covariance matrix Σ^{-1} .

Proposition 2. *When Σ is non degenerate, $\rho = \mathcal{N}(m, \Sigma)$ is the conjugate moment measure of*

$$w(x) = \frac{1}{2}(x - r)^T \Sigma^{-1/3}(x - r),$$

whose Gibbs distribution is $\mathfrak{P}_w = \mathcal{N}(r, \Sigma^{1/3})$ where $r = (I_d + \Sigma^{1/3})^{-1}m$. Potential w is the unique potential for which the Gibbs distribution is Gaussian, satisfying the condition $\nabla w^* \# \mathfrak{P}_w = \rho$.

The proof is similar to that of Proposition 1 and is given in the Appendix. While this potential w may not be the only conjugate moment potential, the Gibbs distribution associated with it, $\mathcal{N}(r, \Sigma^{1/3})$, appears to be better suited to the target distribution ρ . This is particularly evident in the example shown in Figure 1. Additionally, it is worth noting that for the Gaussian case, our factorization still works when ρ is not centered, whereas the approach of Cordero-Erausquin and Klartag (2015) requires ρ to be mean 0.

4 Estimating Conjugate Moment Measures from Data Samples

We first explain how to sample from ρ when its conjugate moment decomposition is known using the Langevin Monte Carlo (LMC) algorithm and a conjugate solver. We then describe a method to estimate a conjugate moment potential of a distribution ρ using i.i.d samples $(x_1, \dots, x_n) \sim \rho$. In this approach, the conjugate moment potential of ρ is parameterized using an input convex neural network (ICNN) w_θ following the architecture proposed in (Vesseron and Cuturi, 2024). The conjugate moment potential w_θ is then estimated using an algorithm inspired by the fixed-point method associated to Theorem 2.

4.1 Sampling from a conjugate moment measure

In this paragraph, we suppose that we know a conjugate moment potential w of ρ , i.e. $\nabla w^* \# \mathfrak{P}_w = \rho$. Knowing w , drawing samples from ρ can be done by first sampling $x_i \sim \mathfrak{P}_w$ and then applying ∇w^* to those points as $\nabla w^*(x_i) \sim \nabla w^* \# \mathfrak{P}_w = \rho$. The LMC algorithm is a widely used method for generating samples from a smooth,

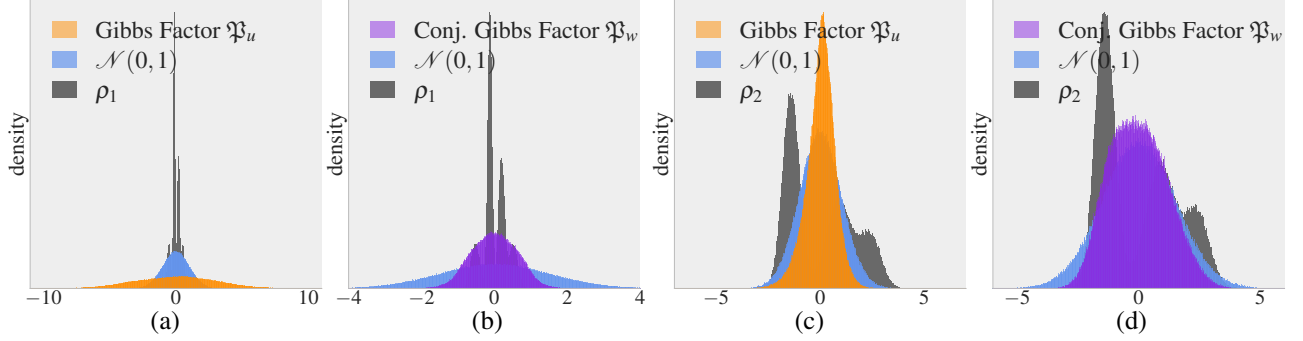


Figure 2: Comparison between the **Gibbs factor** \mathfrak{F}_u and the **conjugate Gibbs factor** \mathfrak{F}_w for two mixtures of 1D Gaussian distributions, ρ_1 and ρ_2 . The density plots overlay the (conjugate) Gibbs factor with ρ and a standard Gaussian distribution $\mathcal{N}(0, 1)$ for reference. Plots (a) and (c) show that the usual Gibbs factor’s spread is inverse to that of ρ . In plots (b) and (d) we see the far more suitable behavior of our conjugate moment factorization.

log-concave density like \mathfrak{F}_w (Roberts and Tweedie, 1996; Cheng and Bartlett, 2018; Dalalyan and Karagulyan, 2019). Starting from an initial point $x^{(0)}$, the LMC algorithm iterates according to the following update rule:

$$x^{(k+1)} = x^{(k)} - \gamma \nabla w(x^{(k)}) + \sqrt{2\gamma} z^{(k)}, \quad z^{(k)} \sim \mathcal{N}(0, I_d).$$

where γ is the step size. After a warm-up period, the LMC iterates are distributed according to the log-concave distribution \mathfrak{F}_w . As for the gradient of the convex conjugate ∇w^* , it can be efficiently estimated from w . By applying Danskin’s envelope theorem (1966), it follows that $\nabla w^*(y)$ is the solution to the following concave maximization problem,

$$\nabla w^*(y) = \arg \sup_x \langle x, y \rangle - w(x).$$

This optimization problem can be solved using algorithms such as gradient ascent, (L)BFGS (Liu and Nocedal, 1989), or ADAM (Kingma and Ba, 2014). Thus, having access to a conjugate moment potential w of ρ enables to efficiently sample from the target distribution ρ . When the conjugate solver is warm-started with $x_0 = y$, gradient steps can be interpreted as a denoising procedure of the Langevin sample.

4.2 Fixed-point Approach

For a probability measure $\rho \in \mathcal{P}(\mathbb{R}^d)$, we define the map $G_\rho : \mathcal{L}(\mathbb{R}) \rightarrow \mathcal{L}(\mathbb{R})$ which to a potential w associates the Brenier potential from ρ to \mathfrak{F}_w

$$G_\rho(w) := \mathfrak{B}(\rho, \mathfrak{F}_w)$$

The fixed point of G_ρ correspond exactly to the conjugate moment potentials of ρ . This observation motivates the following fixed-point iteration scheme to compute a conjugate moment potential of ρ :

$$w_0 := \frac{1}{2} \|\cdot\|^2; \quad \forall t \geq 1, \quad w_{t+1} := G_\rho(w_t).$$

Algorithm 1 Fixed point training of w_θ

- 1: Initialize w_θ such that $w_\theta \approx \frac{1}{2} \|\cdot\|^2$
 - 2: **while** not converged **do**
 - 3: Draw n i.i.d samples $x_i \sim \rho$
 - 4: Draw $y_1, \dots, y_n \sim \mathfrak{F}_{w_\theta}$ using LMC algorithm
 - 5: $\mathcal{L}_\theta \leftarrow \frac{1}{n} \sum_{i=1}^n w_\theta(x_i) - \frac{1}{n} \sum_{i=1}^n w_\theta(\tilde{x}(y_i))$
 - 6: Update w_θ with $\nabla \mathcal{L}_\theta$
 - 7: **end while**
-

Starting from the standard Gaussian distribution $\mathfrak{F}_{w_0} = \mathcal{N}(0, I_d)$, we iteratively compute the OT potential w_{t+1} between the distribution ρ and \mathfrak{F}_{w_t} at iteration $t + 1$. During the next iteration $t + 2$, the updated distribution $\mathfrak{F}_{w_{t+1}}$ becomes the target distribution for computing the next OT map starting from the source ρ . We apply this methodology when the OT map is available in closed form at each step. In all other cases, we found that performing just one optimization step to estimate the OT map at each iteration was sufficient. For this reason, our final methodology relies

on a single ICNN w_θ which serves two purposes at each iteration: generating samples from \mathfrak{P}_{w_θ} and being optimized by doing one step of the neural OT solver from Amos (2023) to approximate the OT map between ρ and \mathfrak{P}_{w_θ} . Algorithm 1 details the steps of the procedure, where $\tilde{x}(y_i)$ is the estimation of $\nabla w_\theta^*(y_i)$, computed as described in Amos (2023).

5 Experiments

We conduct preliminary experiments using the fixed-point iteration scheme described in Section 4.2, focusing on univariate ρ , for which Monge maps have a closed form. Following this, we estimate the conjugate moment potential associated with several 2D distributions as well as the MNIST digits distribution (LeCun et al., 2010).

5.1 Univariate distributions

In the 1D case, the OT map between density functions μ and ν is given by the formula (Peyré et al., 2019):

$$\mathfrak{B}(\mu, \nu) = C_\nu^{-1} \circ C_\mu$$

where $C_\mu : \mathbb{R} \rightarrow [0, 1]$ is the cumulative distribution function associated to μ , defined as: $C_\mu(x) := \int_{-\infty}^x d\mu$. The quantile function $C_\mu^{-1} : [0, 1] \rightarrow \mathbb{R} \cup \{-\infty\}$ is the pseudoinverse $C_\mu^{-1}(r) := \min\{x \in \mathbb{R} \cup \{-\infty\} : C_\mu(x) \geq r\}$. For a given distribution ρ and an initial distribution \mathfrak{P}_{w_0} , the analytical form of the Brenier map enables the exact application of the fixed-point algorithm described in section 4.2. Further implementation details can be found in the Appendix. We use this methodology to compute the moment potential and the *conjugate* moment potential of two distinct mixtures of Gaussians. Display (a) in Figure 2 shows that the Gibbs factor of ρ_1 has a longer tail compared to the centered standard Gaussian. This aligns with theoretical results on Gaussians, which suggest that more concentrated distributions yield broader Gibbs factors. Conversely, for the second measure ρ_2 in (c), which has a larger variance, the Gibbs factor is more concentrated. By design, our *conjugate* Gibbs factor in (b) and (d) closely matches the shapes of ρ_1 and ρ_2 , making it a more suitable prior for generative modeling applications. See also Figure 5 in the appendix, where we display $\nabla u \# \mathfrak{P}_u$ (for the moment potential u) and $\nabla w^* \# \mathfrak{P}_w$ (for the conjugate moment potential w^*) with their respective measures ρ_1 and ρ_2 .

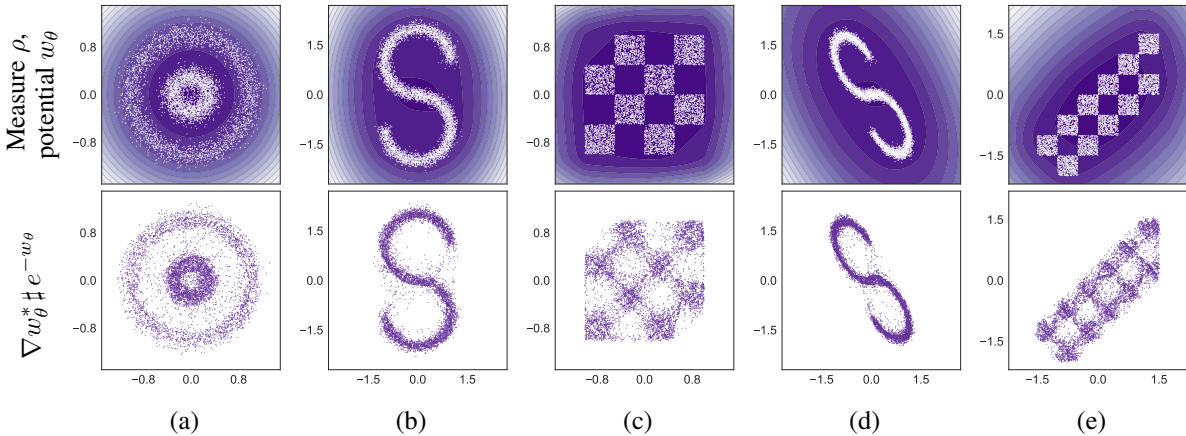


Figure 3: Measure ρ and level sets of its convex conjugate potential w_θ (top), and $\nabla w_\theta^* \# e^{-w_\theta}$ (bottom).

5.2 Generative Modeling

We focus on several 2D distributions as well as the MNIST dataset (LeCun et al., 2010). Our first step is to estimate a conjugate moment potential w for these distributions using the fixed-point method outlined in Section 4.2. Following this, we generate new images based on the conjugate potential w by utilizing the methodology detailed in Section 4.1. The hyperparameters used for these experiments are provided in the Appendix.

2D Experiments. For the 2D distributions: (a) Circles, (b) S-curve, (c) Checkerboard, (d) Scaled-Rotated S-curve and (e) Diag-Checkerboard, the fixed-point approach proved effective. The results, shown in Figure 3, demonstrate that we successfully estimated the conjugate potential associated with these distributions, as the conjugate moment measure of the estimated potential is well aligned with the target distributions ρ . Additionally, in the 2D experiments (c), (d) and (e), we can clearly observe how the Gibbs factor closely follows the shape of the distribution ρ .

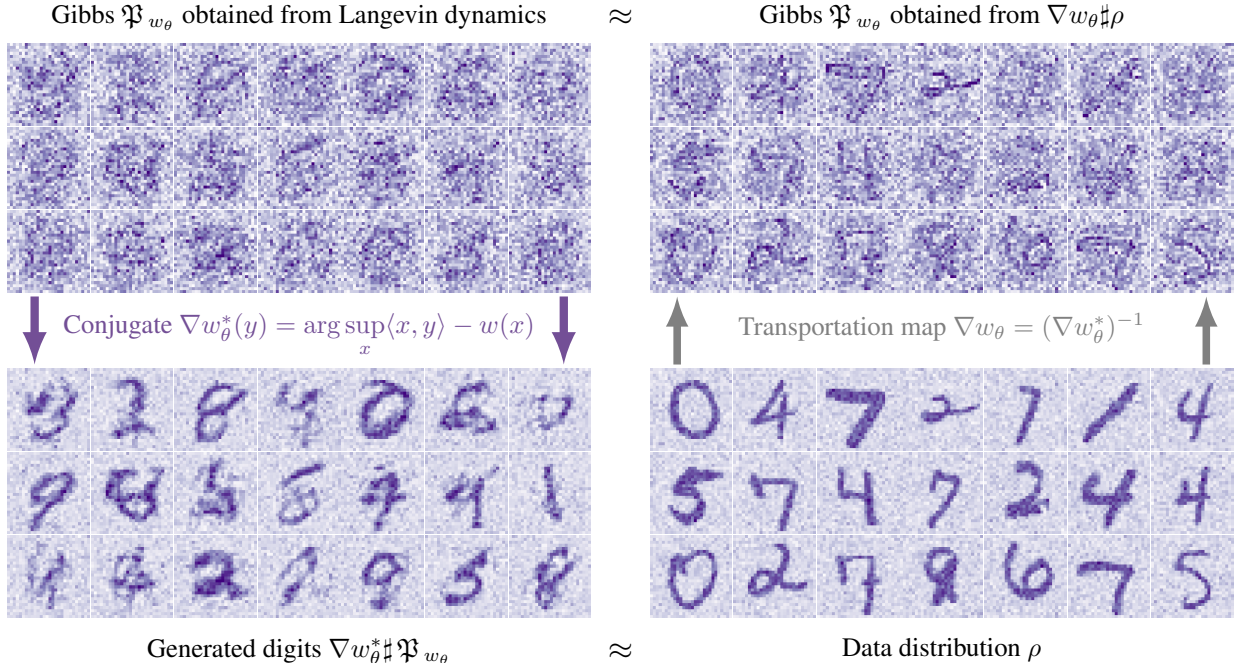


Figure 4: **Learning of the conjugate moment measure.** The single-step generative model ∇w_θ converts highly structured data ρ into a log-concave distribution \mathfrak{P}_{w_θ} . The train distribution ρ is sampled *via optimization*, in an iterative manner. Strict convexity of w_θ guarantees both (i) invertibility of ∇w_θ , and (ii) that Langevin dynamics recovers correctly the conjugate moment \mathfrak{P}_{w_θ} .

MNIST Experiment. The fixed-point method also performs well on the MNIST dataset. As shown in Figure 4, we successfully generated digits using our approach. To the best of our knowledge, this is the first instance where the MNIST distribution has been generated using an ICNN. The structure of the Gibbs distribution, compared to Gaussian noise, seems to facilitate the generative task of transporting \mathfrak{P}_w to the MNIST distribution.

6 Conclusion

In this work, we borrow inspiration from (Cordero-Erausquin and Klartag, 2015; Santambrogio, 2016) to define a new representation for probability measures. For any ρ , we establish the existence of a convex potential w such that $\nabla w^* \# \mathfrak{P}_w = \rho$. We show that this representation is better suited to generative modelling, since the Gibbs factor \mathfrak{P}_w follows more closely the original measure ρ , in contrast to Cordero-Erausquin and Klartag’s approach, $\nabla u \# \mathfrak{P}_u = \rho$, which results in a Gibbs factor \mathfrak{P}_u whose spread is inversely proportional to that of ρ . Our conjugate measure factorization provides a single function w to sample noises (using LMC, guaranteed to work with log-concave distributions) and transform these codes using ∇w^* . We propose to parameterize the conjugate potential w as an ICNN w_θ and rely on the OT toolbox to define a fixed-point iteration scheme to estimate w_θ . While our method demonstrated promising results on generative modeling tasks, its performance is currently hindered by difficulties in training ICNN architecture. Future work may also explore the suitability of replacing $\mathcal{N}(0, I)$ in classic approaches with our pre-trained Gibbs factor \mathfrak{P}_w .

Acknowledgements

This work was performed using HPC resources from GENCI–IDRIS (Grant 2023-103245).

References

Brandon Amos. On amortizing convex conjugates for optimal transport. In *The Eleventh International Conference on Learning Representations*, 2023.

- Brandon Amos, Lei Xu, and J Zico Kolter. Input convex neural networks. In *International Conference on Machine Learning*, pages 146–155. PMLR, 2017.
- Shiri Artstein-Avidan, Bo’az Klartag, and Vitali Milman. The santaló point of a function, and a functional form of the santaló inequality. *Mathematika*, 51(1-2):33–48, 2004.
- Ball. Isometric problems in ℓ_p and sections of convex sets. *Thesis (Ph.D.), University of Cambridge*, 1986.
- Yann Brenier. Polar factorization and monotone rearrangement of vector-valued functions. *Communications on pure and applied mathematics*, 44(4):375–417, 1991.
- Ricky TQ Chen, Yulia Rubanova, Jesse Bettencourt, and David K Duvenaud. Neural ordinary differential equations. *Advances in neural information processing systems*, 31, 2018.
- Xiang Cheng and Peter Bartlett. Convergence of langevin mcmc in kl-divergence. In *Algorithmic Learning Theory*, pages 186–211. PMLR, 2018.
- Dario Cordero-Erausquin and Bo’az Klartag. Moment measures. *Journal of Functional Analysis*, 268(12):3834–3866, 2015.
- Arnak S Dalalyan and Avetik Karagulyan. User-friendly guarantees for the langevin monte carlo with inaccurate gradient. *Stochastic Processes and their Applications*, 129(12):5278–5311, 2019.
- John M Danskin. The theory of max-min, with applications. *SIAM Journal on Applied Mathematics*, 14(4):641–664, 1966.
- Matthias Gelbrich. On a formula for the l2 wasserstein metric between measures on euclidean and hilbert spaces. *Mathematische Nachrichten*, 147(1):185–203, 1990. doi: <https://doi.org/10.1002/mana.19901470121>. URL <https://onlinelibrary.wiley.com/doi/abs/10.1002/mana.19901470121>.
- Ian Goodfellow, Jean Pouget-Abadie, Mehdi Mirza, Bing Xu, David Warde-Farley, Sherjil Ozair, Aaron Courville, and Yoshua Bengio. Generative adversarial nets. *Advances in neural information processing systems*, 27, 2014.
- Will Grathwohl, Ricky TQ Chen, Jesse Bettencourt, Ilya Sutskever, and David Duvenaud. Ffjord: Free-form continuous dynamics for scalable reversible generative models. *arXiv preprint arXiv:1810.01367*, 2018.
- Jonathan Ho, Ajay Jain, and Pieter Abbeel. Denoising diffusion probabilistic models. In H. Larochelle, M. Ranzato, R. Hadsell, M.F. Balcan, and H. Lin, editors, *Advances in Neural Information Processing Systems*, volume 33, pages 6840–6851. Curran Associates, Inc., 2020. URL https://proceedings.neurips.cc/paper_files/paper/2020/file/4c5bcfec8584af0d967f1ab10179ca4b-Paper.pdf.
- Diederik P Kingma and Jimmy Ba. Adam: A method for stochastic optimization. *arXiv preprint arXiv:1412.6980*, 2014.
- Diederik P. Kingma and Max Welling. Auto-Encoding Variational Bayes. In *2nd International Conference on Learning Representations, ICLR 2014, Banff, AB, Canada, April 14-16, 2014, Conference Track Proceedings*, 2014.
- Alexander Korotin, Vage Egiazarian, Arip Asadulaev, Alexander Safin, and Evgeny Burnaev. Wasserstein-2 generative networks. In *International Conference on Learning Representations*, 2020.
- Yann LeCun, Corinna Cortes, and CJ Burges. Mnist handwritten digit database. *ATT Labs [Online]*. Available: <http://yann.lecun.com/exdb/mnist>, 2, 2010.
- Dong Bok Lee, Dongchan Min, Seanie Lee, and Sung Ju Hwang. Meta-GMVAE: Mixture of gaussian VAE for unsupervised meta-learning. In *International Conference on Learning Representations*, 2021. URL <https://openreview.net/forum?id=wSOUFjsNYjn>.
- Chen Liang, Wenguan Wang, Jiaxu Miao, and Yi Yang. Gmmseg: Gaussian mixture based generative semantic segmentation models. *Advances in Neural Information Processing Systems*, 35:31360–31375, 2022.
- Yaron Lipman, Ricky T. Q. Chen, Heli Ben-Hamu, Maximilian Nickel, and Matthew Le. Flow matching for generative modeling. In *The Eleventh International Conference on Learning Representations*, 2023.
- Dong C Liu and Jorge Nocedal. On the limited memory bfgs method for large scale optimization. *Mathematical programming*, 45(1-3):503–528, 1989.
- Ashok Makkuva, Amirhossein Taghvaei, Sewoong Oh, and Jason Lee. Optimal transport mapping via input convex neural networks. In *International Conference on Machine Learning*, pages 6672–6681. PMLR, 2020.
- Gaspard Monge. Mémoire sur la théorie des déblais et des remblais. *Histoire de l’Académie Royale des Sciences*, pages 666–704, 1781.
- Gabriel Peyré, Marco Cuturi, et al. Computational optimal transport: With applications to data science. *Foundations and Trends® in Machine Learning*, 11(5-6):355–607, 2019.

- Aram-Alexandre Pooladian, Heli Ben-Hamu, Carles Domingo-Enrich, Brandon Amos, Yaron Lipman, and Ricky TQ Chen. Multisample flow matching: Straightening flows with minibatch couplings. *arXiv preprint arXiv:2304.14772*, 2023.
- Gareth O. Roberts and Richard L. Tweedie. Exponential convergence of Langevin distributions and their discrete approximations. *Bernoulli*, 2(4):341 – 363, 1996.
- Filippo Santambrogio. Optimal transport for applied mathematicians. *Birkäuser, NY*, 55(58-63):94, 2015.
- Filippo Santambrogio. Dealing with moment measures via entropy and optimal transport. *Journal of Functional Analysis*, 271(2):418–436, 2016. ISSN 0022-1236. doi: <https://doi.org/10.1016/j.jfa.2016.04.009>. URL <https://www.sciencedirect.com/science/article/pii/S0022123616300507>.
- Yang Song, Jascha Sohl-Dickstein, Diederik P Kingma, Abhishek Kumar, Stefano Ermon, and Ben Poole. Score-based generative modeling through stochastic differential equations. In *International Conference on Learning Representations*, 2020.
- Jakub Tomczak and Max Welling. Vae with a vampprior. In *International conference on artificial intelligence and statistics*, pages 1214–1223. PMLR, 2018.
- Alexander Tong, Nikolay Malkin, Guillaume Huguët, Yanlei Zhang, Jarrid Rector-Brooks, Kilian Fatras, Guy Wolf, and Yoshua Bengio. Improving and generalizing flow-based generative models with minibatch optimal transport. *arXiv preprint arXiv:2302.00482*, 2023.
- Nina Vesseron and Marco Cuturi. On a neural implementation of brenier’s polar factorization. In *International Conference on Machine Learning*, pages 49434–49454. PMLR, 2024.

A Appendix / Supplementary Material

A.1 Proof of Proposition 1

Let us observe that ρ is the moment measure of u if and only if ∇u is the Monge map from \mathfrak{P}_u to ρ . One can then consider quadratic functions $u_{r,\Delta}(x) = \frac{1}{2}(x-r)^T \Delta^{-1}(x-r)$ whose Gibbs distribution is $\mathfrak{P}_u = \mathcal{N}(r, \Delta)$ and use the expression (Gelbrich, 1990) of the OT map between two Gaussian distributions $\mathcal{N}(m_A, \Sigma_A)$ and $\mathcal{N}(m_B, \Sigma_B)$:

$$T_{m_A, \Sigma_A, m_B, \Sigma_B} : x \mapsto m_B + M(x - m_A)$$

where $M = \Sigma_A^{-1/2}(\Sigma_A^{1/2} \Sigma_B \Sigma_A^{1/2})^{1/2} \Sigma_A^{-1/2}$, to solve the equation

$$\nabla u_{r,\Delta}(x) = T_{r,\Delta,0,\Sigma}(x) \quad \forall x \in \mathbb{R}^d$$

One get:

$$\Delta^{-1}(x-r) = M(x-r) \quad \text{with } M = \Delta^{-1/2}(\Delta^{1/2} \Sigma \Delta^{1/2})^{1/2} \Delta^{-1/2}$$

By identification, we obtain that $\Delta^{-1} = M = \Delta^{-1/2}(\Delta^{1/2} \Sigma \Delta^{1/2})^{1/2} \Delta^{-1/2}$ which leads to $\Delta = \Sigma^{-1}$. It means that the functions in $\{u_{r,\Sigma^{-1}}, r \in \mathbb{R}^d\}$ are fixed-point of G_ρ with $\rho = \mathcal{N}(0, \Sigma)$. According to Cordero-Erausquin and Klartag (2015), the moment potential is unique up to translation, which implies that there are no other convex functions whose moment measure is ρ . This observation can be intuitively understood from equation 8 where the term $\ln(\int e^{-u} \int e^{-u^*})$ is constant, equal to $n \ln(2\pi)$ for centered multivariate normal distributions. Among these distributions, the optimal solution involves selecting u such that $\mathfrak{P}_{u^*} = \rho$ in order to minimize the KL divergence term.

A.2 Proof of Proposition 2

The proof is similar to the proof of Proposition 1. Given $\rho = \mathcal{N}(m, \Sigma)$, we are looking for w such that $\nabla w^* \# \mathfrak{P}_w = \rho$ and $\mathfrak{P}_w = \mathcal{N}(r, \Delta)$. This means that $w(x) = \frac{1}{2}(x-r)^T \Delta^{-1}(x-r)$ and $w^*(x) = \frac{1}{2}x^T \Delta x + x^T r$. Moreover $\nabla w^* : x \rightarrow \Delta x + r$ must be the OT map between $\mathfrak{P}_w = \mathcal{N}(r, \Delta)$ and $\rho = \mathcal{N}(m, \Sigma)$. The OT map between these two gaussians is known in closed form and is given by $x \rightarrow m + M(x-r)$ with $M = \Delta^{-1/2}(\Delta^{1/2} \Sigma \Delta^{1/2})^{1/2} \Delta^{-1/2}$. Solving $\Delta = \Delta^{-1/2}(\Delta^{1/2} \Sigma \Delta^{1/2})^{1/2} \Delta^{-1/2}$ gives $\Delta = \Sigma^{1/3}$ while solving $r = m - Mr$ gives $r = (I_d + \Sigma^{1/3})^{-1}m$. We conclude that ρ is the conjugate moment measure of the unique potential w among those whose Gibbs distribution is Gaussian.

A.3 Proof Theorem 2

Let ρ be an absolutely continuous probability measure supported on a compact, convex set $\Omega \subset \mathbb{R}^d$. Ω being compact, it is bounded and there exists a real number R such that Ω be included in the ball $\mathcal{B}(0, R)$. We begin by recalling Schauder's fixed point theorem, which is central to our proof for showing that G_ρ^Ω , defined as:

$$G_\rho^\Omega(v) := \mathfrak{B}(\rho, \mathfrak{P}_v^\Omega)$$

where \mathfrak{P}_v^Ω the probability measure with density

$$\frac{e^{-v(x)} \mathbf{1}_{x \in \Omega}}{\int_\Omega e^{-v(z)} dz},$$

admits a fixed-point.

Theorem (Schauder's fixed point Theorem). *Let $(X, \|\cdot\|)$ be a Banach space and $\mathcal{M} \subset X$ is compact, convex, and nonempty. Any continuous operator $A : \mathcal{M} \rightarrow \mathcal{M}$ has at least one fixed point.*

We consider the Banach space $X = (\mathcal{C}(\Omega), \|\cdot\|_\infty)$ to study the continuity of G_ρ^Ω on the set

$$\mathcal{M} = \{f \in \mathcal{C}(\Omega) \text{ such that } \forall x, y \in \Omega, |f(x) - f(y)| \leq R\|x - y\|_2 \text{ and } f(0_{\mathbb{R}^d}) = 0\}.$$

We prove the two following lemmas in order to use Schauder's theorem.

Lemma 1. *The set \mathcal{M} is a non-empty, compact, convex set of X .*

Lemma 2. *G_ρ^Ω is well defined and continuous on \mathcal{M} and $G_\rho^\Omega(\mathcal{M}) \subseteq \mathcal{M}$.*

By applying these two lemmas along with Schauder's theorem, we conclude that G_ρ^Ω has a fixed point v_{opt} in $\mathcal{M} \subset \mathcal{C}(\Omega)$. Moreover, the absolute continuity of $\mathfrak{P}_{v_{\text{opt}}}^\Omega$ ensures that the optimal solution v_{opt} whose gradient transports ρ onto $\mathfrak{P}_{v_{\text{opt}}}^\Omega$ is strictly convex on the support of ρ , Ω . Additionally, the gradient of its Legendre transform ∇v_{opt}^* is the OT map from $\mathfrak{P}_{v_{\text{opt}}}^\Omega$ to ρ .

A.3.1 Proof of Lemma 1.

\mathcal{M} is non-empty 0 is included in \mathcal{M} which is therefore not empty.

\mathcal{M} is convex Let f and g functions of \mathcal{M} and $\lambda \in [0, 1]$. We have that $\lambda f + (1 - \lambda)g \in \mathcal{C}(\Omega)$ and that $\lambda f(0) + (1 - \lambda)g(0) = 0$. Let $x \in \Omega$ and $y \in \Omega$, then :

$$\begin{aligned} |(\lambda f(x) + (1 - \lambda)g(x)) - (\lambda f(y) + (1 - \lambda)g(y))| &\leq \lambda|f(x) - f(y)| + (1 - \lambda)|g(x) - g(y)| \\ &\leq \lambda R\|x - y\|_2 + (1 - \lambda)R\|x - y\|_2 = R\|x - y\|_2 \end{aligned}$$

where, for the first inequality, we rely on the fact that the absolute value verifies the triangular inequality and for the second inequality, we use that f and g belong to \mathcal{M} and are therefore R -lipschtiz.

\mathcal{M} is compact We rely on Arzela-Ascoli theorem which is recalled below to show that the set \mathcal{M} is compact. We also recall the definitions of equicontinuity and equiboundedness.

Definition. A family of functions $\mathcal{F} \subset \mathcal{C}(\Omega)$ is equibounded if there exists a constant C_0 such that for all $x \in \Omega$ and $f \in \mathcal{F}$, we have $|f(x)| \leq C_0$.

Definition. A family of functions $\mathcal{F} \subset \mathcal{C}(\Omega)$ is equicontinuous if for all $\varepsilon > 0$, there exists δ such that for $x, y \in \Omega$,

$$\|x - y\| < \delta \implies \forall f \in \mathcal{F} |f(x) - f(y)| < \varepsilon$$

Theorem (Arzela-Ascoli). Let (K, d) a compact space, a family of functions $\mathcal{F} \subset \mathcal{C}(K)$ is relatively compact if and only if \mathcal{F} is equibounded and equicontinuous.

The family of functions \mathcal{M} is equibounded. In fact, for $f \in \mathcal{M}$ and $x \in \Omega$, we have that:

$$|f(x)| = |f(x) - f(0)| \leq R\|x - 0\|_2 \leq R^2$$

The first equality comes from the fact that $f \in \mathcal{M}$, therefore $f(0) = 0$, the first inequality uses the fact that f is Lipschitz continuous with constant R while the last one is due to the fact that $x \in \Omega \subset B(0, R)$.

The family of functions \mathcal{M} is equicontinuous. For $\varepsilon > 0$, we define $\delta = \frac{\varepsilon}{R}$. Let $f \in \mathcal{M}$ and $x, y \in \Omega$ such that $\|x - y\|_2 < \delta$ then because f is Lipschitz on Ω , we have that

$$|f(x) - f(y)| \leq R\|x - y\|_2 < R\delta = \varepsilon.$$

Then, according to Arzela-Ascoli theorem, \mathcal{M} is relatively compact i.e. its closure is compact.

\mathcal{M} is closed in $X = (\mathcal{C}(\Omega), \|\cdot\|_\infty)$ Let (f_n) be a sequence of functions in \mathcal{M} that converges uniformly to a limiting function f . We have that $f \in \mathcal{C}(\Omega)$ which is closed. Moreover, because (f_n) converges uniformly to f , it also converges pointwise and in particular $f_n(0) = 0 \rightarrow 0 = f(0)$. Finally, because $\forall n, f_n$ is Lipschitz continuous, we have

$$|f_n(x) - f_n(y)| \leq R\|x - y\|_2 \forall n$$

By taking the limit when $n \rightarrow +\infty$ we get that:

$$|f(x) - f(y)| \leq R\|x - y\|_2$$

and f is Lipschitz continuous with constant R and $f \in \mathcal{M}$. This proves that \mathcal{M} is closed and that \mathcal{M} is therefore compact.

A.3.2 Proof of Lemma 2.

G_ρ^Ω is well-defined on \mathcal{M} For a given $v \in \mathcal{M}$, the fact that $v \in \mathcal{C}(\Omega)$ and that Ω is non-negligible (because ρ is an absolutely continuous probability measure supported on Ω) ensure the measure \mathfrak{P}_v^Ω to be well-defined. Using Brenier's theorem, the absolute continuity of ρ garantees the existence of the Brenier potential $\mathfrak{B}(\rho, \mathfrak{P}_v^\Omega)$ and the fact that G_ρ^Ω is therefore well-defined on the set $\mathcal{M} \subset \mathcal{C}(\Omega)$.

$G_\rho^\Omega(\mathcal{M}) \subset \mathcal{M}$ For a given $v \in \mathcal{M}$, the Brenier potential $G_\rho^\Omega(v)$ verifies $G_\rho^\Omega(v)(0) = 0$ by definition. As a convex function which takes real values on Ω , $G_\rho^\Omega(v)$ is continuous on Ω and $G_\rho^\Omega(v) \in \mathcal{C}(\Omega)$. Moreover, the gradient of the obtained potential $\nabla G_\rho^\Omega(v)$ transports ρ on \mathfrak{P}_v^Ω . The probability measures \mathfrak{P}_v^Ω and ρ are both compactly supported on $\Omega \subset B(0, R)$ which implies that the support of the optimal transport plan $\gamma = (i_d, \nabla G_\rho^\Omega(v))_{\#}\rho$ is included in

$\Omega \times \Omega$. Ω being the support of ρ , we have that for each $x \in \Omega$, $\nabla G_\rho^\Omega(v)(x) \in \Omega \subset B(0, R)$ and in particular $\|\nabla G_\rho^\Omega(v)(x)\|_2 \leq R$. Ω being convex and $G_\rho^\Omega(v)$ being differentiable in the interior of Ω , we can apply the mean value theorem to deduce that:

$$\forall x, y \in \Omega \quad |G_\rho^\Omega(v)(x) - G_\rho^\Omega(v)(y)| \leq \sup_{z \in \Omega} \|\nabla G_\rho^\Omega(v)(z)\|_2 \|x - y\|_2 \leq R \|x - y\|_2$$

$G_\rho^\Omega(v)$ is therefore Lipschitz continuous with constant R and it belongs to the set \mathcal{M} .

G_ρ^Ω is continuous on \mathcal{M} To prove the continuity of G_ρ^Ω on \mathcal{M} , one can remark that $G_\rho^\Omega = H_\rho \circ F^\Omega$, with

$$\begin{aligned} F^\Omega : \mathcal{M} &\longrightarrow \mathcal{N} \\ v &\longrightarrow \mathfrak{P}_v^\Omega \end{aligned}$$

and

$$\begin{aligned} H_\rho : \mathcal{N} &\longrightarrow \mathcal{C}(\Omega) \\ \mu &\longrightarrow \mathfrak{B}(\rho, \mu) \end{aligned}$$

with $\mathcal{N} = \{\mathfrak{P}_v^\Omega, v \in \mathcal{C}(\Omega)\} \subset \mathcal{C}(\Omega)$. We show that both function F^Ω and H_ρ are continuous in $X = (\mathcal{C}(\Omega), \|\cdot\|_\infty)$. Let $v \in \mathcal{C}(\Omega)$ and (v_n) a family of functions of $\mathcal{C}(\Omega)$ that converges uniformly to v . We will show that the family $(F^\Omega(v_n))$ converges uniformly to $F^\Omega(v)$. Let x in Ω and $n \in \mathbb{N}$, we have:

$$\begin{aligned} |F^\Omega(v_n)(x) - F^\Omega(v)(x)| &= \left| \frac{e^{-v_n(x)}}{\int_\Omega e^{-v_n(z)} dz} - \frac{e^{-v(x)}}{\int_\Omega e^{-v(z)} dz} \right| \\ &= \left| \frac{(e^{-v_n(x)} \int_\Omega e^{-v(z)} dz) - (e^{-v(x)} \int_\Omega e^{-v_n(z)} dz)}{\int_\Omega e^{-v_n(z)} dz \int_\Omega e^{-v(z)} dz} \right| \end{aligned}$$

We will use the following lemma:

Lemma 3. *If (v_n) converges uniformly to v in $\mathcal{C}(\Omega)$ with Ω compact then e^{-v_n} converges uniformly to e^{-v} in $\mathcal{C}(\Omega)$.*

Proof of Lemma 3. Let us denote by f the real function $f : x \longrightarrow e^{-x}$. f is continuous on \mathbb{R} . Because $v \in \mathcal{C}(\Omega)$ and Ω compact, we have, by Heine's theorem, that $v(\Omega) \subset \mathbb{R}$ is compact and therefore bounded. There exists a and b such that $v(\Omega) \subseteq [a, b]$. Moreover because (v_n) converges uniformly to v , there exists N such that $n \geq N \implies v_n(\Omega) \subseteq [a - 1, b + 1]$. f being continuous on \mathbb{R} , it is uniformly continuous on the interval $[a - 1, b + 1]$ according to Heine's theorem. We deduce that $(f(v_n))$ converges uniformly to $f(v)$. \square

On the other hand, the function $g : t \longrightarrow e^{-v(t)}$ is continuous on the compact Ω as a composition of continuous functions. By Heine's theorem, the image of Ω by g is a compact and there exists $c, \ell \in \mathbb{R}^{+*}$ such that $g(\Omega) \subset [c, \ell]$ with $c > 0$. Because e^{-v_n} converges uniformly to e^{-v} in $\mathcal{C}(\Omega)$, there exists N_0 such that $n \geq N_0 \implies e^{-v_n}(z) \geq \frac{c}{2} \forall z \in \Omega$. As a consequence, we have for $n \geq N_0$:

$$\int_\Omega e^{-v_n(z)} dz \int_\Omega e^{-v(z)} dz \geq \int_\Omega \frac{c}{2} dz \int_\Omega c dz = \frac{c^2}{2} |\Omega|^2$$

with $|\Omega|$ the lebesgue measure of the compact Ω . Ω being non-negligible, we have $|\Omega| > 0$. Let $C_0 = \frac{2}{c^2 |\Omega|^2}$, we have shown that for $n \geq N_0$ we had:

$$\left| \frac{1}{\int_\Omega e^{-v_n(z)} dz \int_\Omega e^{-v(z)} dz} \right| < C_0$$

Furthermore, one notes that:

$$\begin{aligned}
& \left| \left(e^{-v_n(x)} \int_{\Omega} e^{-v(z)} dz \right) - \left(e^{-v(x)} \int_{\Omega} e^{-v_n(z)} dz \right) \right| \\
&= \left| \left(e^{-v_n(x)} \int_{\Omega} e^{-v(z)} dz \right) - \left(e^{-v(x)} \int_{\Omega} e^{-v(z)} dz \right) + \left(e^{-v(x)} \int_{\Omega} e^{-v(z)} dz \right) - \left(e^{-v(x)} \int_{\Omega} e^{-v_n(z)} dz \right) \right| \\
&\leq \left| \left(e^{-v_n(x)} - e^{-v(x)} \right) \int_{\Omega} e^{-v(z)} dz \right| + \left| e^{-v(x)} \left(\int_{\Omega} e^{-v(z)} dz - \int_{\Omega} e^{-v_n(z)} dz \right) \right| \\
&\leq \left| e^{-v_n(x)} - e^{-v(x)} \right| \ell |\Omega| + \ell \left| \int_{\Omega} e^{-v(z)} dz - \int_{\Omega} e^{-v_n(z)} dz \right| \\
&\leq \|e^{-v_n} - e^{-v}\|_{\infty} \ell |\Omega| + \ell \int_{\Omega} |e^{-v(z)} - e^{-v_n(z)}| dz \\
&\leq 2\ell |\Omega| \|e^{-v_n} - e^{-v}\|_{\infty}
\end{aligned}$$

Until now, we have shown that for $n \geq N_0$ we had, for $x \in \Omega$:

$$|F^{\Omega}(v_n)(x) - F^{\Omega}(v)(x)| \leq C_0 2\ell |\Omega| \|e^{-v_n} - e^{-v}\|_{\infty}$$

Let $\varepsilon > 0$, let us define $\varepsilon_0 = \frac{\varepsilon}{C_0 2\ell |\Omega|} > 0$. Because (e^{-v_n}) converges uniformly to e^{-v} , there exists N_1 such that $n \geq N_1 \implies \|e^{-v_n} - e^{-v}\|_{\infty} < \varepsilon_0$. Let us denote $N = \max(N_0, N_1)$, we have that for $n \geq N$,

$$|F^{\Omega}(v_n)(x) - F^{\Omega}(v)(x)| \leq \varepsilon$$

Because this is true for any $x \in \Omega$, we have $\|F^{\Omega}(v_n) - F^{\Omega}(v)\|_{\infty} \leq \varepsilon$. We just proved that F^{Ω} is continuous at v for any $v \in \mathcal{C}(\Omega)$ ie F^{Ω} is continuous on $\mathcal{C}(\Omega)$ and in particular it is continuous on $\mathcal{M} \subset \mathcal{C}(\Omega)$.

We will now show that H_{ρ} is continuous on \mathcal{N} . Let $\mu \in \mathcal{N}$ and let (μ_n) a family of densities from \mathcal{N} that converges uniformly to μ . For $n \in \mathbb{N}$, we denote by $\mathcal{P}(\mu_n)$ and $\mathcal{P}(\mu)$ the probability measures associated to the respective densities μ_n and μ . Because (μ_n) converges uniformly to μ , we have that $\mathcal{P}(\mu_n)$ converges in distribution to $\mathcal{P}(\mu)$. Then according to Santambrogio (2015) (Theorem 1.52), the family of Kantorovich potentials from ρ to $\mathcal{P}(\mu_n)$ with value 0 in 0 that we denote (f_n^*) converges uniformly to the Kantorovich potential f^* from ρ to $\mathcal{P}(\mu)$ whose value is 0 in 0. Therefore, the family of Brenier potentials $(H_{\rho}(\mu_n) : t \rightarrow \frac{1}{2} \|t\|^2 - f_n^*(t))$ converges uniformly to $H_{\rho}(\mu) = \frac{1}{2} \|\cdot\|^2 - f^*$. We conclude that H_{ρ} is continuous on \mathcal{N} and by composition of continuous functions G_{ρ}^{Ω} is continuous on \mathcal{M} .

A.4 1D Experiments

We conducted two experiments, with ρ defined as a mixture of Gaussian distributions. In the first experiment, ρ is a mixture of four Gaussians: $\mathcal{N}(-0.1, 0.07)$, $\mathcal{N}(0.3, 0.1)$, $\mathcal{N}(0.3, 0.1)$, $\mathcal{N}(0.7, 0.15)$ with mixture weights $\frac{1}{7}, \frac{3}{7}, \frac{2}{7}, \frac{1}{7}$, respectively. In the second experiment, ρ is a mixture of the three Gaussians $\mathcal{N}(-0.8, 0.4)$, $\mathcal{N}(1.5, 0.6)$, $\mathcal{N}(3, 0.5)$, with weights $\frac{1}{2}, \frac{1}{3}, \frac{1}{6}$. To approximate these mixtures, we used 400,000 samples and estimated their histograms using 100,000 bins. This allowed us to compute the cumulative distribution and quantile functions using numpy's `cumsum` and `quantile` functions, which were essential for estimating the OT map at each iteration of the fixed-point algorithm. The algorithm converged after 300 iterations. Figure 5 illustrates that, in both experiments, the moment measures $\nabla u \# \mathfrak{P}_u$ and the conjugate moment measures $\nabla w^* \# \mathfrak{P}_w$ of the computed potentials perfectly align with ρ_i confirming that the fixed-point algorithm successfully identified moment potentials u and conjugate moment potentials w of ρ_i .

A.5 Hyperparameters and infrastructure

For the MNIST experiment, we used MNIST dataset (LeCun et al., 2010) under the terms of the Creative Commons Attribution-Share Alike 3.0 license. In this experiment, we convolve the MNIST images with Gaussian noise of standard deviation 0.3 to ensure that the OT map from the MNIST distribution to the log-concave distribution \mathfrak{P}_w exists, as this is guaranteed when the starting distribution is absolutely continuous (Santambrogio, 2015). This effect is visible in Figure 4.

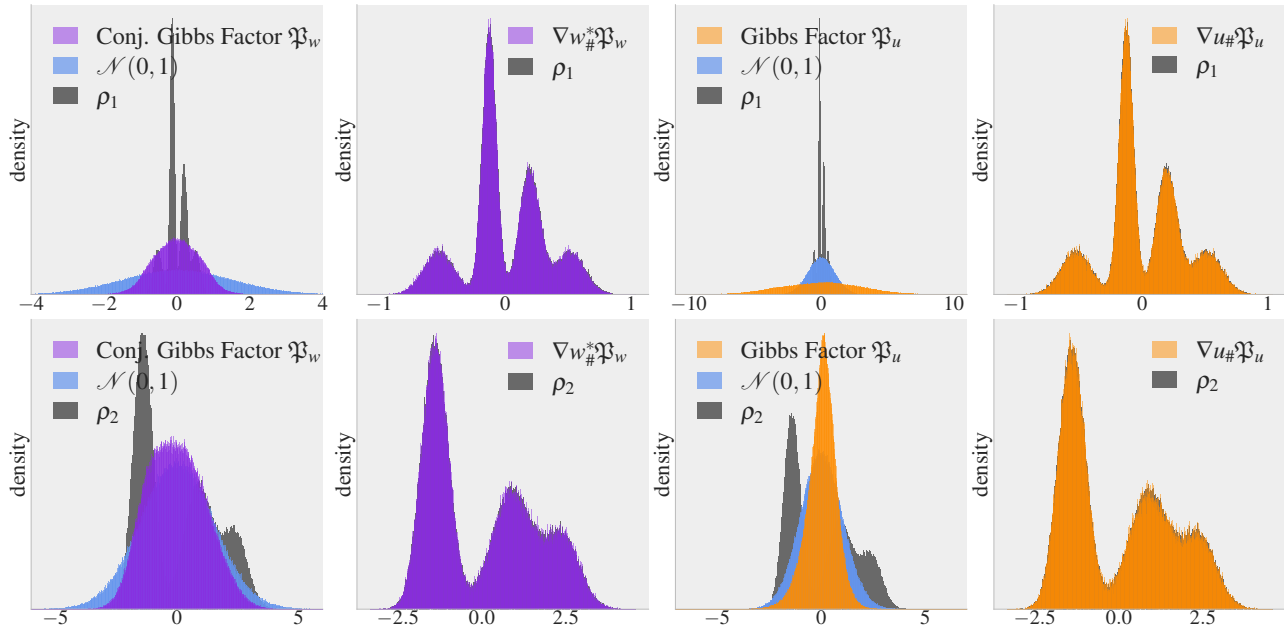


Figure 5: Convergence of the fixed-point algorithm.

All runs have been made on single GPU V100 or A100-40GB. All the experiments in Figure 3 were generated using a common set of hyperparameters, detailed in Table 1. The number of particles used (i.e., batch size) and the chosen step size γ in the LMC process vary across experiments. For the 2D distributions Circles, S-curve, and Scaled-Rotated S-curve, we used 1024 particles, while for Checkerboard and Diag-Checkerboard, a larger number of particles (4096) was used to ensure the stability of the algorithm. The step size γ used in the LMC process depends on the shape of the log concave distribution $\mathfrak{P}_{w_\theta^*}$. Specifically, we used a step size of $5e-5$ for Circles, $1e-4$ for S-curve and Scaled-Rotated S-curve, and $1e-3$ for Checkerboard and Diag-Checkerboard.

The hyperparameters used for the MNIST experiments are given in Table 2. To determine these hyperparameters, we used commonly applied architectures for ICNNs and conducted a grid search over γ testing values $1e-3$, $5e-4$, $1e-4$, $5e-5$ and $1e-5$, as well as for the learning rate of w_θ , considering values $1e-3$, $5e-4$ and $1e-4$. We adopt the approach of Amos (2023), where the cost of computing the conjugate at each training step is amortized by initializing the conjugate solver with the predictions of an MLP. This MLP is trained via regression on the outputs of the conjugate solver. The MLP consists of three hidden layers with 128 units each for the 2D experiments and three hidden layers with 256 units each for the MNIST experiment. It is trained using the Adam optimizer with default parameters, and a fixed learning rate of $1e-4$ for the 2D experiments and $5e-4$ for the MNIST experiment. It is important to note that the number of LMC steps listed in the tables refers to the steps taken to sample from \mathfrak{P}_{w_θ} starting from uniform noise, as used to generate the figures. During training, however, we reuse the particles sampled from the previous gradient step and apply 200 LMC steps to these particles to form the new batch.

Hyperparameter	Value
w_θ architecture	dense 2 → 128 → 128 → 128 → 128 → 128 → 1 ELU activation functions
w_θ optimizer	Adam step size = 0.0001 $\beta_1 = 0.5$ $\beta_2 = 0.5$
Conjugate solver w_θ^*	Adam step size with cosine decay schedule init value = 0.1 alpha = 1e-4 $\beta_1 = 0.9$ $\beta_2 = 0.999$ 100 iterations
Langevin sampling	number of steps = 6000 (=200 during training)
number of gradient steps	700,000

Table 1: Hyperparameters for the 2D experiments of Figure 3.

Hyperparameter	Value
w_θ architecture	dense 2 → 512 → 512 → 512 → 512 → 512 → 1 ELU activation functions
w_θ optimizer	Adam step size = 0.0005 $\beta_1 = 0.5$ $\beta_2 = 0.5$
Conjugate solver w_θ^*	Adam step size with cosine decay schedule init value = 0.1 alpha = 1e-4 $\beta_1 = 0.9$ $\beta_2 = 0.999$ 100 iterations
Langevin sampling	step size $\gamma = 0.001$ number of steps = 6000 (=200 during training)
number of gradient steps	100,000
batch size	512

Table 2: Hyperparameters for the MNIST experiment of Figure 4.